

More Large N limits of 3d gauge theories

Louise Anderson^a,

*The Blackett Laboratory, Imperial College London,
Prince Consort Road, London SW7 2AZ, United Kingdom*

and Nadav Drukker^b

*Department of Mathematics, King's College London,
The Strand, London WC2R 2LS, United Kingdom*

Abstract

In this paper we study the large N solution to matrix models describing the partition functions of 3d supersymmetric gauge theories on \mathbb{S}^3 . The model we focus on has a single $U(N)$ gauge group and fundamental fields, whose number scales with N , also known as the Veneziano limit. The novel point in our model is our choice of masses for the fundamental fields. Instead of vanishing or fixed masses, we consider a linear distribution. We show that the model can still be solved by standard large N techniques and explore the different phases of the model. We also comment about other natural mass distributions.

^alouise.m.a.anderson@imperial.ac.uk

^bnadav.drukker@gmail.com

1 Introduction

The tools of supersymmetric localization [1] have revolutionized the study of supersymmetric field theories. They allow one, under very restrictive assumptions, to reduce the infinite dimensional path integral of a field theory on certain manifolds to a finite dimensional integral. One of the most important applications has been to test dualities, as the partition functions of two dual models should be the same. Most often the resulting integral expressions are not identical, but are equal after using some integral identities.

This is a great achievement, but it is not the same as actually calculating the partition function. In the most celebrated case, that of 4d $\mathcal{N} = 2$ theories on \mathbb{S}^4 , the resulting integral is extremely complicated - it is equivalent to a calculation in a 2d CFT, via the AGT correspondence [2, 3] - but explicit evaluation of the integrals is not available even for $SU(2)$ groups (Liouville theory).

In this paper we study the matrix model for 3d theories on \mathbb{S}^3 [4]. The case of the ABJ(M) model and other circular quivers has received a lot of attention and the matrix model has been solved for many such cases either in the large N limit, sometimes to all orders in $1/N$ and in a select few cases exactly [5–8]. For linear quivers the case of small N (with no Chern-Simons term) can be solved completely explicitly by rather elementary integration [9], but the large N limit is more complicated.

We study a model with $\mathcal{N} = 3$ SUSY comprising of a single $U(N)$ node with K flavours. The partition function of the theory on \mathbb{S}^3 is given by the matrix model [10]

$$Z = \frac{1}{N!} \int d^N z \frac{\prod_{i < j} \text{sh}^2(z_i - z_j)}{\prod_{i=1}^N \prod_{k=1}^K \text{ch}(z_i - m_k)} e^{2\pi i \zeta \sum_i z_i + \pi i \kappa \sum_i z_i^2}. \quad (1.1)$$

where m_i are K arbitrary masses, ζ is the Fayet-Iliopoulos (FI) parameter and κ the Chern-Simons (CS) level. The FI term can be eliminated by a shift of the integration variables and the masses m_k , and therefore will henceforth be ignored.

We consider this model in the large N and large K limit, also known as the Veneziano limit, which raises the question of how to choose the K mass parameters. In [11, 12] this model was studied with all vanishing masses or taking two values $\pm M$. The purpose of this note is to show that this model has a nice large N solution also when the masses are distributed along an interval. We choose the linear distribution

$$m_k = m_1 + \frac{k-1}{K-1} \mu, \quad (1.2)$$

and solve the model in the large N limit.

The planar solution of the matrix model has the eigenvalues z_i distributed along a cut (we only consider single cut solutions, which is consistent with numerical checks), and we find an interesting interplay between the distribution of eigenvalues and the mass distribution. In the absence of a CS term, the eigenvalues are centered around the masses with two possibilities: The width of the eigenvalue distribution may be larger or smaller than that of the masses. The CS term provides an extra force attracting the eigenvalues to the origin and if the masses are not distributed symmetrically, this leads to further configurations with partial overlap or no overlap of the eigenvalues and the mass distribution.

The rest of the note is organised as follows: In the next section we solve the model. In Section 3 we plot some graphs of eigenvalue distributions and investigate their possible forms. In Section 4

we study the model in the limit of large \mathbb{S}^3 radius, where it simplifies dramatically and where the different possible overlaps of the masses and eigenvalue density outlined above correspond to different phases with a rich structure of third order phase transitions. We conclude with a discussion.

2 Solving the matrix model

To solve the matrix model (1.1), we first change variables

$$Z_i = C e^{2\pi z_i}, \quad M_k = C e^{2\pi m_k}, \quad (2.1)$$

where C is an arbitrary constant. Similarly, if the eigenvalues z_i are supported on the interval $[a, b]$, then the exponentiated eigenvalues $Z_i = C e^{2\pi z_i}$ are supported on $[A, B]$. The partition function is now

$$\begin{aligned} Z &= \frac{\prod_{k=1}^K M_k^{N/2}}{(2\pi)^N N!} \int d^N Z \prod_{i<j} (Z_i - Z_j)^2 \frac{\prod_{i=1}^N Z_i^{K/2-N} e^{i\frac{\kappa}{4\pi} \log^2(Z_i/C)}}{\prod_{i=1}^N \prod_{k=1}^K (Z_i + M_k)} \\ &= \frac{1}{N!} \int d^N Z \prod_{i<j} (Z_i - Z_j)^2 e^{-N \sum_{i=1}^N V(Z_i)}, \end{aligned} \quad (2.2)$$

with the potential

$$\begin{aligned} V(Z) &= C_0 + \frac{1}{N} \sum_{k=1}^K \log(Z + M_k) - \left(\frac{K}{2N} - 1\right) \log \frac{Z}{C} - i \frac{\kappa}{4\pi N} \log^2 \frac{Z}{C}, \\ C_0 &= \frac{1}{N} \log(2\pi) - \left(\frac{K}{2N} - 1\right) \log C - \frac{1}{2N} \sum_{k=1}^K \log M_k. \end{aligned} \quad (2.3)$$

The saddle point equation for an eigenvalue Z_i is

$$2 \sum_{j \neq i} \frac{1}{Z_i - Z_j} = NV'(Z_i) = \sum_{k=1}^K \frac{1}{Z_i + M_k} - \left(\frac{K}{2} - N\right) \frac{1}{Z_i} - i \frac{\kappa}{2\pi} \frac{\log(Z_i/C)}{Z_i}, \quad (2.4)$$

We want to study this model in the large N limit, where the saddle point approximation becomes exact, and we are then faced with choosing a distribution for the masses. As mentioned in the introduction, we focus on the simple choice of a constant distribution of masses between m_1 and m_K according to (1.2).

As we take the large N limit, it is useful to introduce the Veneziano parameter

$$\chi = \frac{K}{2N}, \quad (2.5)$$

as well as the 't Hooft coupling

$$\lambda = \frac{N}{\kappa}, \quad (2.6)$$

and then take the large N limit in such a way that both these parameters are kept fixed. Therefore, in this limit we have

$$\begin{aligned} \frac{1}{N} \sum_{k=1}^K \log(Z + M_k) &\rightarrow \frac{\chi}{\pi(m_K - m_1)} \int_{M_1}^{M_K} \frac{dM}{M} \log(Z + M) \\ &= 2\chi \log Z - \frac{2\chi}{2\pi\mu} \left(\text{Li}_2 \left(-\frac{M_K}{Z} \right) - \text{Li}_2 \left(-\frac{M_1}{Z} \right) \right). \end{aligned} \quad (2.7)$$

The force resulting from the full potential is

$$-V'(Z) = \frac{1}{Z} \left(\frac{2\chi}{2\pi\mu} \log \frac{Z + M_K}{Z + M_1} + \frac{i}{2\pi\lambda} \log Z - \left(\chi + 1 + \frac{i}{2\pi\lambda} \log C \right) \right). \quad (2.8)$$

In order to find the eigenvalue distribution, we use the standard technique and introduce the resolvent $\omega(Z)$ defined by

$$\omega(Z) = \oint dZ' \frac{\rho(Z')}{Z - Z'} \quad (2.9)$$

Assuming that the eigenvalues are distributed along a single cut, then for a generic function $V'(Z)$, the resolvent is given by

$$\omega(Z) = \frac{1}{2} \oint_{\mathcal{C}} \frac{dZ' V'(Z')}{2\pi i Z - Z'} \sqrt{\frac{(Z - A)(Z - B)}{(Z' - A)(Z' - B)}} \quad (2.10)$$

where \mathcal{C} is the path around the branch cut between A and B . From this, one can then obtain the density by studying the discontinuity across the branch cut

$$\rho(Z) = -\frac{1}{2\pi i} (\omega(Z + i\epsilon) - \omega(Z - i\epsilon)). \quad (2.11)$$

We rewrite equation (2.10) as

$$\omega(Z) = \frac{1}{2} V'(Z) - \frac{1}{2} M(Z) \sqrt{(Z - A)(Z - B)}, \quad (2.12)$$

where M is defined by the integral over a deformation of the contour \mathcal{C} to one that encircles ∞

$$M(Z) = \oint_{\infty} \frac{dZ' V'(Z')}{2\pi i Z' - Z} \frac{1}{\sqrt{(Z' - A)(Z' - B)}}. \quad (2.13)$$

Our expression for the force includes poles and terms of the form $\frac{\log(Z+M)}{Z}$. It is convenient to consider their contribution to the resolvent independently.

Adapting the solution of the Chern-Simons matrix model [13, 14] to a generic logarithmic term

$$V'(Z) = \frac{\log(Z + M)}{Z}, \quad (2.14)$$

gives

$$M_{\log}(Z) = \frac{1}{2\pi i} \oint_{\infty} dZ' \frac{\log(Z' + M)}{Z'(Z' - Z) \sqrt{(Z' - A)(Z' - B)}}. \quad (2.15)$$

The contour is such that we get a contribution from the logarithmic branch cut and from the pole at $Z' = 0$ (but not from $Z' = Z$), resulting in

$$\begin{aligned}
M_{\log}(Z) &= - \int_{-\infty}^{-M} dZ' \frac{1}{Z'(Z' - Z)\sqrt{(Z' - A)(Z' - B)}} - \frac{\log M}{Z\sqrt{AB}} \\
&= \frac{2}{Z\sqrt{AB}} \log \frac{\sqrt{A} + \sqrt{B}}{\sqrt{B(A+M)} + \sqrt{A(B+M)}} \\
&\quad + \frac{1}{Z\sqrt{(Z-A)(Z-B)}} \log \frac{\left(\sqrt{(A-Z)(B+M)} - \sqrt{(B-Z)(A+M)}\right)^2}{(M+Z)(\sqrt{A-Z} - \sqrt{B-Z})^2}.
\end{aligned} \tag{2.16}$$

The contribution of the pole term is much simpler. For

$$V'(Z) = \frac{1}{Z}, \tag{2.17}$$

we find

$$M_{\text{pole}}(Z) = -\frac{1}{Z\sqrt{AB}}. \tag{2.18}$$

Combining all those and the usual Chern-Simons terms together gives

$$\begin{aligned}
\omega(Z) &= \frac{1}{2Z} \left(\chi + 1 + \frac{i}{2\pi\lambda} \log C \right) \left(1 + \frac{\sqrt{(A-Z)(B-Z)}}{\sqrt{AB}} \right) \\
&\quad - \frac{\sqrt{(A-Z)(B-Z)}}{Z\sqrt{AB}} \left(\frac{\chi}{\pi\mu} \log \frac{\sqrt{B(A+M_K)} + \sqrt{A(B+M_K)}}{\sqrt{B(A+M_1)} + \sqrt{A(B+M_1)}} - \frac{i}{2\pi\lambda} \log \frac{2\sqrt{AB}}{\sqrt{A} + \sqrt{B}} \right) \\
&\quad + \frac{\chi}{2\pi\mu Z} \left(\log \frac{\left(\sqrt{(A-Z)(B+M_K)} - \sqrt{(B-Z)(A+M_K)}\right)^2}{\left(\sqrt{(A-Z)(B+M_1)} - \sqrt{(B-Z)(A+M_1)}\right)^2} - \log \frac{(Z+M_K)^2}{(Z+M_1)^2} \right) \\
&\quad + \frac{i}{4\pi\lambda Z} \log \frac{\left(\sqrt{A(Z-B)} - \sqrt{B(Z-A)}\right)^2}{Z^2 (\sqrt{Z-A} - \sqrt{Z-B})^2}.
\end{aligned} \tag{2.19}$$

2.1 Asymptotic behaviour of the resolvent

Expanding $\omega(Z) = \omega^{(0)} + \omega^{(1)}/Z + \mathcal{O}(Z^{-2})$, the requirement that $\omega^{(0)} = 0$ can be expressed as:

$$\chi + 1 + \frac{i}{\pi\lambda} \log \frac{\sqrt{C}(\sqrt{A} + \sqrt{B})}{2\sqrt{AB}} = \frac{2\chi}{\pi\mu} \log \frac{\sqrt{B(A+M_K)} + \sqrt{A(B+M_K)}}{\sqrt{B(A+M_1)} + \sqrt{A(B+M_1)}}. \tag{2.20}$$

The condition $\omega^{(1)} = 1$ can be recast as $\omega^{(1)} + \frac{A+B}{2}\omega^{(0)} = 1$ which gives

$$-\chi + 1 + \frac{i}{\pi\lambda} \log \frac{\sqrt{A} + \sqrt{B}}{2\sqrt{C}} = \frac{2\chi}{\pi\mu} \log \frac{\sqrt{A+M_K} - \sqrt{B+M_K}}{\sqrt{A+M_1} - \sqrt{B+M_1}}. \tag{2.21}$$

For $\kappa \neq 0$, *i.e.* finite λ , we can choose C to simplify these equations. For $\lambda \rightarrow \infty$, the C -dependence drops out.

We can use (2.20) to simplify the resolvent (2.19)

$$\begin{aligned}
\omega(Z) &= \frac{1}{2Z} \left(\chi + 1 + \frac{i}{2\pi\lambda} \log C \right) \\
&+ \frac{\chi}{2\pi\mu Z} \left(\log \frac{\left(\sqrt{(A-Z)(B+M_K)} - \sqrt{(B-Z)(A+M_K)} \right)^2}{\left(\sqrt{(A-Z)(B+M_1)} - \sqrt{(B-Z)(A+M_1)} \right)^2} - \log \frac{(Z+M_K)^2}{(Z+M_1)^2} \right) \\
&+ \frac{i}{4\pi\lambda Z} \log \frac{\left(\sqrt{A(Z-B)} - \sqrt{B(Z-A)} \right)^2}{Z^2 (\sqrt{Z-A} - \sqrt{Z-B})^2}.
\end{aligned} \tag{2.22}$$

This expression still depends on A and B , but there is no easy way to solve (2.20) and (2.21) to simplify this further, and need to keep those two constraints in mind below.

2.2 The eigenvalue density

The exponentiated eigenvalues Z are supported on the interval $[A, B]$, and their density is proportional to the discontinuity in ω . This comes from $\sqrt{(A-Z)(B-Z)}$, leading to

$$\begin{aligned}
\rho(Z) &= -\frac{i}{2\pi^2\lambda Z} \arctan \frac{(\sqrt{B}-\sqrt{A})\sqrt{(Z-A)(B-Z)}}{\sqrt{A}(B-Z) + \sqrt{B}(Z-A)} \\
&+ \frac{\chi}{\pi^2\mu Z} \left[\arctan \sqrt{\frac{(B-Z)(A+M_K)}{(Z-A)(B+M_K)}} - \arctan \sqrt{\frac{(B-Z)(A+M_1)}{(Z-A)(B+M_1)}} \right].
\end{aligned} \tag{2.23}$$

We can easily go back to the original variables z by the relation $\rho(z)dz = \rho(Z)dZ = 2\pi Z\rho(Z)dz$, and equation (2.1). We furthermore return to the original mass variables m_i by the replacement $\mu = m_K - m_1$. This all gives us the expression for $\rho(z)$ as

$$\begin{aligned}
\rho(z) &= -\frac{i}{\pi\lambda} \arctan \frac{\sqrt{\text{sh}(z-a)\text{sh}(b-z)}}{\text{ch}\left(\frac{a+b-2z}{2}\right)} \\
&+ \frac{2\chi}{\pi(m_K - m_1)} \left[\arctan \sqrt{\frac{\text{sh}(b-z)\text{ch}(a-m_K)}{\text{sh}(z-a)\text{ch}(b-m_K)}} - \arctan \sqrt{\frac{\text{sh}(b-z)\text{ch}(a-m_1)}{\text{sh}(z-a)\text{ch}(b-m_1)}} \right],
\end{aligned} \tag{2.24}$$

where the interval endpoints a, b may be fixed by the normalisation conditions, or, equivalently, from the condition on the asymptotic behaviour of the resolvent (equations (2.20) and (2.21)).

2.3 Wilson loops

The vacuum expectation value of Wilson loops [15] around a big circle of the \mathbb{S}^3 may be computed as [4]

$$W = \left\langle \frac{1}{N} \sum_i e^{2\pi z_i} \right\rangle \xrightarrow{N \rightarrow \infty} \int dz \rho(z) e^{2\pi z}. \tag{2.25}$$

It turns out that this is easier to evaluate in the exponentiated variable Z , and it then takes the form

$$W = \frac{1}{C} \oint dZ Z \omega(Z) = \frac{1}{C} \int_A^B dZ Z \rho(Z). \quad (2.26)$$

Carrying out this integration, we find

$$W = -\frac{i(\sqrt{A} - \sqrt{B})^2}{8\pi C \lambda} - \frac{\chi}{2\pi C \mu} \left(M_K - M_1 - \sqrt{(A + M_K)(B + M_K)} + \sqrt{(A + M_1)(B + M_1)} \right) \quad (2.27)$$

or, expressed in the original variables

$$W = -\frac{i}{8\pi\lambda} e^{\pi(a+b)} \operatorname{sh}^2\left(\frac{b-a}{2}\right) - \frac{\chi}{2\pi(m_K - m_1)} \left[e^{\pi(m_K + m_1)} \operatorname{sh}(m_K - m_1) - e^{\frac{\pi(a+b)}{2}} \left(e^{\pi m_K} \sqrt{\operatorname{ch}(a - m_K) \operatorname{ch}(b - m_K)} - e^{\pi m_1} \sqrt{\operatorname{ch}(a - m_1) \operatorname{ch}(b - m_1)} \right) \right]. \quad (2.28)$$

2.4 Symmetric distributions

In the special case of a symmetric mass distribution and vanishing FI-parameter, the entire problem has reflection symmetry around the origin. This means that $a = -b$, and so, the equations simplify

$$\rho(z) = -\frac{i}{\pi\lambda} \arctan \frac{\sqrt{\operatorname{ch}^2(b) - \operatorname{ch}^2(z)}}{\operatorname{ch}(z)} + \frac{\chi}{\pi m} \arctan \frac{\operatorname{sh}(m) \sqrt{\operatorname{ch}^2(b) - \operatorname{ch}^2(z)}}{\operatorname{ch}(z) \sqrt{\operatorname{ch}^2(b) + \operatorname{sh}^2(m)}}. \quad (2.29)$$

The condition (2.20) now takes the form

$$\chi - 1 = \frac{i}{\pi\lambda} \log \frac{\operatorname{ch}(b)}{2} + \frac{\chi}{\pi m} \log \frac{\sqrt{\operatorname{ch}^2(b) + \operatorname{sh}^2(m)} + \operatorname{sh}(m)}{\operatorname{ch}(b)}, \quad (2.30)$$

and we can use it to fix $b(m, \lambda, \chi)$. (2.21) is then automatically satisfied.

The Wilson loop (2.28) is

$$W = -\frac{i}{8\pi\lambda} \operatorname{sh}^2(b) - \frac{\chi}{4\pi m} \operatorname{sh}(m) \left(\operatorname{ch}(m) - \sqrt{\operatorname{ch}^2(b) + \operatorname{sh}^2(m)} \right). \quad (2.31)$$

3 Form of the solution

In this section we study the different forms the eigenvalue density can take. We plot the analytic expressions for varying values of the parameters and compare it to a numerical analysis of the solution to the saddle point equations with $N = 100$. The analytic expressions provide a good fit to the numerical results for the entire range of the parameters we tested (with negative imaginary 't Hooft coupling).

Figure 1 shows the regime of large μ , where the eigenvalue density approaches a constant. In this case, $m_K - m_1 = 20$ is not very large, so we see a few eigenvalues along the tails extending

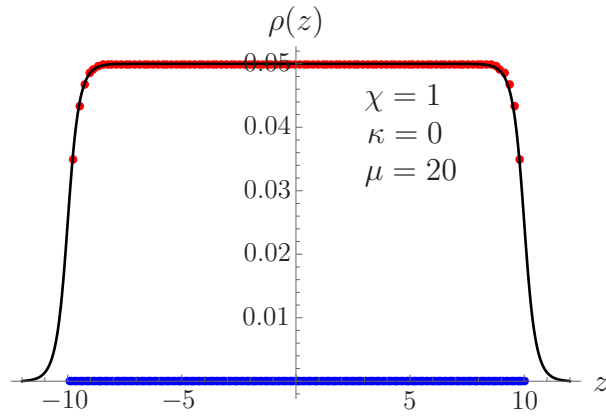


Figure 1: The eigenvalue density for vanishing CS-level, $K = 2N$ ($\chi = 1$) and a relatively large $\mu = 20$. The black line is the analytic density, and the red dots are numerical results for $N = 100$. The blue dots are the distribution of masses, here condensed to a line.

beyond the range of the masses $[-10, 10]$. The limit of large μ is studied in detail in the next section.

When μ is small the eigenvalue distribution forms a bell shape, as can be seen in the left graph in Figure 2. As we increase μ , as in the right graph, the bell widens until it becomes flat, like in Figure 1.

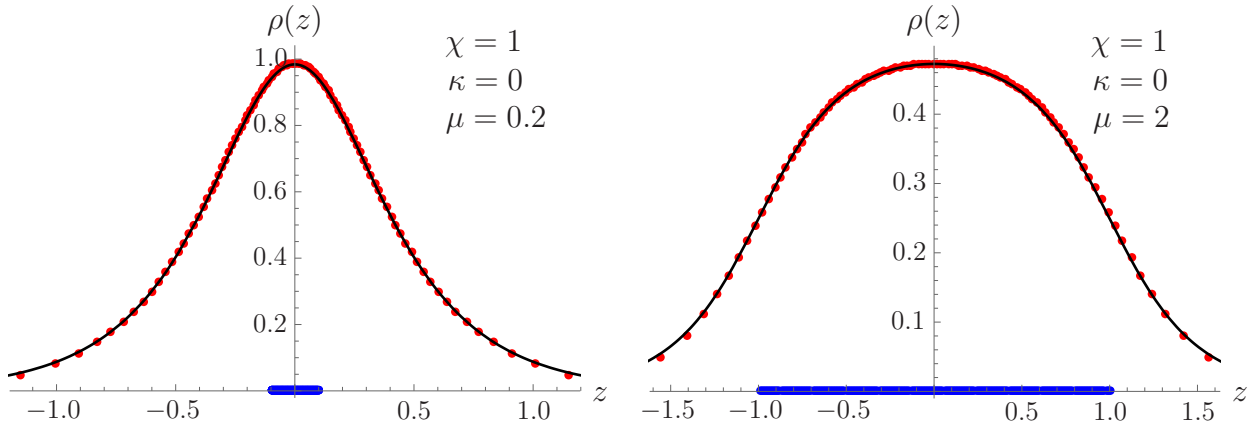


Figure 2: The eigenvalue density for vanishing CS-level, $K = 2N$ ($\chi = 1$) and varying μ smaller than in Figure 1.

The eigenvalues get squeezed further towards the origin if we increase χ (or K). In the absence of a CS term, the matrix model does not converge for $\chi < 1$, but it can increase arbitrarily. In Figure 3 we illustrate the case of $\chi = 2$ with the same values of μ as in Figure 2. We see that with large enough μ and/or χ , the eigenvalues no longer extend beyond the range of the mass distribution.

To check when this happens, we can solve for $b = m_K$, which also fixes $a = m_1$, as we are in

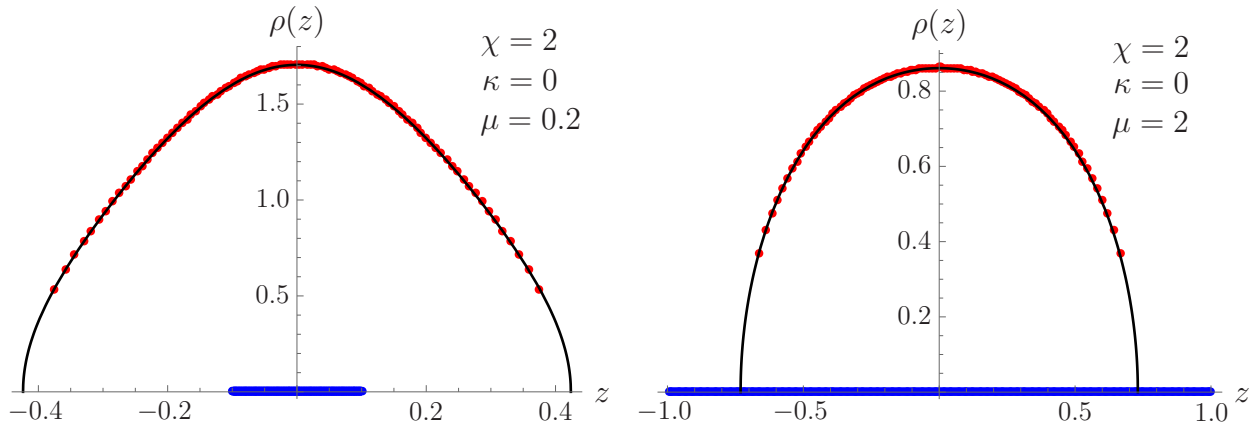


Figure 3: The eigenvalue density for vanishing CS-level, $K = 4N$ ($\chi = 2$) and the same two values of μ as in Figure 2.

the symmetric case, discussed in Section 2.4. Equation (2.30) then gives

$$\chi - 1 = \frac{i}{\pi\lambda} \log \frac{\text{ch}(m)}{2} + \frac{\chi}{\pi m} \log \frac{\sqrt{2 \text{ch}(2m)} + \text{sh}(m)}{\text{ch}(m)}, \quad (3.1)$$

In particular, if we focus on the case of $\kappa = 0$, as in the above examples, we find a simple curve of $\chi(m)$, shown in Figure 4. It is easy to see that there are no discontinuities when crossing this line, so it does not lead to a phase transition. Those arise in the next section, when we consider the decompactification limit.

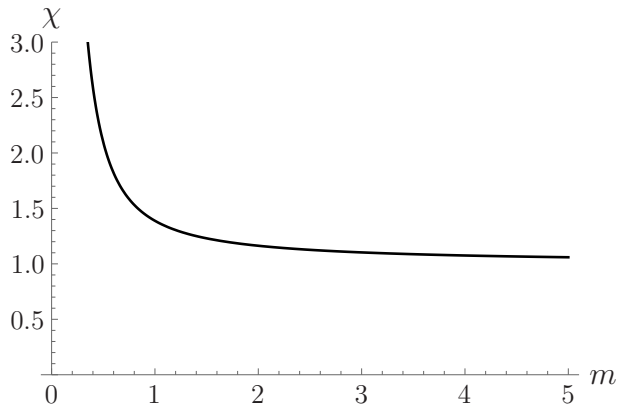


Figure 4: The values of χ for which $b = m_K$ for symmetric mass distributions and $\kappa = 0$.

The Chern-Simons coupling adds an extra potential term pushing the eigenvalues towards the origin, and in fact with a nonzero CS parameter we can take $\chi \rightarrow 0$. Some plots with imaginary CS terms are shown in Figure 5.

The condition that the endpoints of the eigenvalue distribution coincide with the endpoints of the masses (3.1) now leads to a hypersurface in 3d.

The situation gets more complicated when the mass distribution is not centered around the origin. In the absence of a CS term, the eigenvalue distribution translates with the masses, but

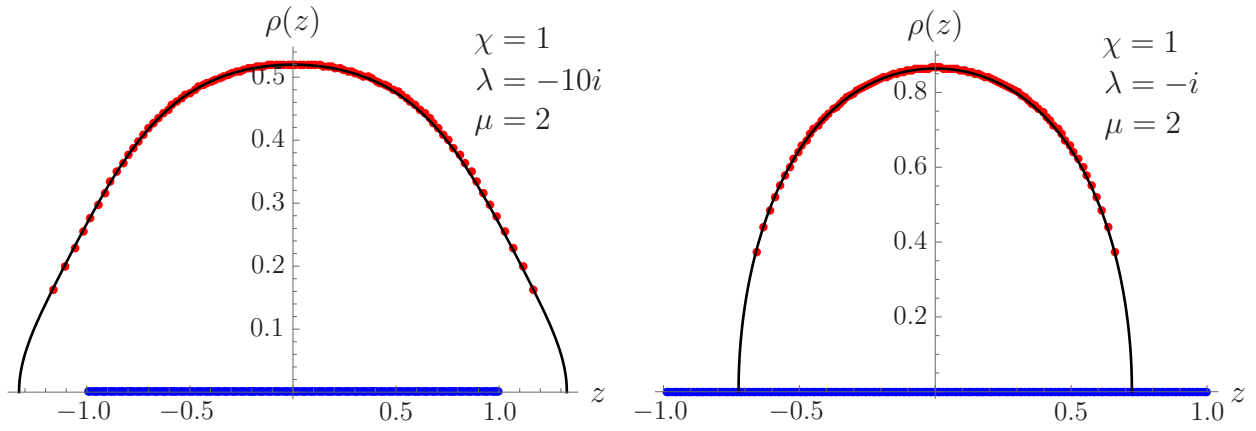


Figure 5: Eigenvalue densities with varying CS-level.

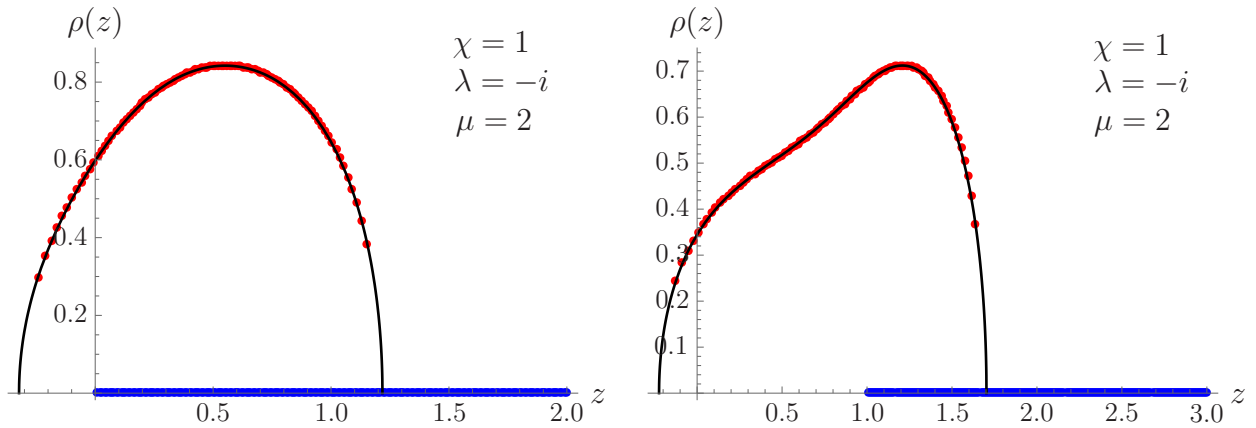


Figure 6: Asymmetrical eigenvalue densities arising in the presence of nonzero CS-level and a mass distribution shifted relative to the right graph in Figure 5 by 1 (left) and 2 (right).

the CS term breaks translation symmetry, and tends to keep the eigenvalues centred around the origin. Two graphs illustrating this are shown in Figure 6. One can see that it may now be possible for one endpoint of the eigenvalue distributions to be outside of the domain of the masses, while the other is still inside. Depending on the range of the parameters, any order among a , b , m_1 and m_K consistent with $a < b$ and $m_1 < m_K$ is possible. Indeed, increasing the value of m_1 a bit beyond that in the right graph in Figure 6 leads to the eigenvalues completely disjoint from the mass distribution: $a < b < m_1 < m_K$.

4 The decompactification limit and phase transitions

Non-trivial phase structures has been observed previously for mass-deformed theories in 3, 4 and 5 dimensions [11, 12, 16–23]. It stands to reason that something similar might occur here. Therefore, we would like to examine the behaviour of the free energy and Wilson loops in the so-called decompactification limit where we take the radius R of the \mathbb{S}^3 to infinity while keeping κ and λ/R fixed. To that end we reintroduce the explicit radius dependance in the original matrix model

(1.1) (in which the radius of the sphere was taken to be unity) via the substitution

$$m_j \rightarrow Rm_j, \quad z_j \rightarrow Rz_j. \quad (4.1)$$

The saddle point equation for the eigenvalue z_i (with $\zeta = 0$) now takes the form

$$\frac{1}{N} \sum_{j \neq i} \coth(\pi R(z_i - z_j)) = \frac{\chi}{K} \sum_{k=1}^K \tanh(\pi R(z_i - m_k)) - \frac{i}{\lambda} Rz_i. \quad (4.2)$$

In the limit $R \rightarrow \infty$, the hyperbolic functions approach sign-functions of the real part of the argument. Let us introduce $\tilde{\lambda} = i\frac{\lambda}{R}$ which is held fixed (and positive) as $R \rightarrow \infty$. Going to the continuum limit, where the masses are distributed according to $\rho_m(m)$, we then find

$$\int_a^b dz' \rho(z') \text{sign}(z - z') = \chi \int_{m_1}^{m_K} dm \rho_m(m) \text{sign}(z - m) + \frac{1}{\tilde{\lambda}} z. \quad (4.3)$$

Differentiating both sides with respect to z gives us the relation

$$\rho(z) = \chi \rho_m(z) + \frac{1}{2\tilde{\lambda}}. \quad (4.4)$$

This is a remarkably simple expression for the eigenvalue density, which is valid for arbitrary mass distributions ρ_m , and not only the constant one which we analyzed previously for finite R . This equation is not enough, though, to determine the endpoints a and b .

To that end, consider (4.3) for $z = a$ and $z = b$

$$-1 = 2\chi \int_{m_1}^a dm \rho_m(m) - \chi + \frac{1}{\tilde{\lambda}} a, \quad 1 = 2\chi \int_{m_1}^b dm \rho_m(m) - \chi + \frac{1}{\tilde{\lambda}} b. \quad (4.5)$$

We are interested in phase transitions as we change the parameter χ and coupling λ . These arise when $\rho(z)$ changes discontinuously and it is easy to see that for continuous ρ_m , the solution to (4.4) subject to the constraints in (4.5) will depend continuously on χ and λ .

Phase transitions arise then from discontinuities in ρ_m , and focusing again on the case of constant mass-density, the discontinuities are at the endpoints m_1 and m_K . Given that $m_1 < m_K$ and $a < b$, there are six possible arrangements of these variables.

4.1 Symmetric mass distributions

Before analyzing the general case, let us focus on symmetric mass distributions $m_K = -m_1 = m$, which imply also $a = -b$. In this case there are two possible phases with $b < m$ and $b > m$. It is clear from (4.5), that the interface is at

$$1 = \chi + \frac{m}{\tilde{\lambda}}. \quad (4.6)$$

This matches the large R limit of (3.1), where the last term drops out. Note that since $\tilde{\lambda} > 0$, this phase transition only occurs for $\chi < 1$.

The case of $b < m$ leads to a constant eigenvalue density $\rho(z) = \frac{\chi}{2m} + \frac{1}{2\tilde{\lambda}}$ on the interval $[-b, b]$ and clearly $b = \frac{1}{2\rho(0)}$. This happens in the domain where $\tilde{\lambda} < \frac{m}{1-\chi}$.

For $b > m$, or $\tilde{\lambda} > \frac{m}{1-\chi}$ the eigenvalue density is

$$\rho(z) = \begin{cases} \frac{1}{2\tilde{\lambda}} + \frac{\chi}{2m}, & -m < z < m, \\ \frac{1}{2\tilde{\lambda}}, & m < |z| < b, \\ 0, & |z| > b, \end{cases} \quad (4.7)$$

and $b = \tilde{\lambda}(1 - \chi)$.

We can evaluate the free energy on both sides of the phase transition. For a given $\rho_m(m)$ and $\rho(z)$ it is given in this limit by

$$F = \log N! - \pi N^2 R \left[\int dz dz' \rho(z) \rho(z') |z - z'| - 2\chi \int dz dm \rho(z) \rho_m(m) |z - m| - \frac{1}{\tilde{\lambda}} \int dz \rho(z) z^2 \right]. \quad (4.8)$$

We thus find

$$F = \log N! + \begin{cases} \pi N^2 R \left(m\chi - \frac{m\lambda}{3(m+\lambda\chi)} \right), & \tilde{\lambda} < \frac{m}{1-\chi}, \\ \pi N^2 R \left(m\chi - \frac{m\lambda}{3(m+\lambda\chi)} - \frac{\chi}{3\lambda(\lambda\chi+m)} (\lambda(1-\chi) - m)^3 \right), & \tilde{\lambda} > \frac{m}{1-\chi}. \end{cases} \quad (4.9)$$

Clearly this is continuous at $b = m$, and so are the first and second derivatives with respect to $\tilde{\lambda}$ or χ or m , so this is a third order phase transition.

Similarly, the Wilson loop may be computed by (2.25), giving

$$W = \begin{cases} \frac{(\tilde{\lambda}\chi+m)}{4\pi\tilde{\lambda}mR} \operatorname{sh} \left(\frac{2\tilde{\lambda}mR}{\lambda\chi+m} \right), & \tilde{\lambda} < \frac{m}{1-\chi}, \\ \frac{\chi}{4\pi mR} \operatorname{sh}(2mR) + \frac{1}{4\pi\lambda R} \operatorname{sh} \left(2\tilde{\lambda}(1-\chi)R \right), & \tilde{\lambda} > \frac{m}{1-\chi}. \end{cases} \quad (4.10)$$

Unlike the free energy, this has a discontinuity already in the second derivative. Since we are in the large R limit we can replace all sh functions with exp and away from the phase boundary can also ignore the subleading exponent in the second phase, so

$$W \simeq \begin{cases} \frac{(\tilde{\lambda}\chi+m)}{4\pi\tilde{\lambda}mR} e^{2\pi\tilde{\lambda}mR/(\lambda\chi+m)}, & \tilde{\lambda} < \frac{m}{1-\chi}, \\ \frac{\chi}{4\pi mR} e^{2\pi mR}, & \tilde{\lambda} > \frac{m}{1-\chi}, \end{cases} \quad (4.11)$$

which, just as the free energy, is continuous at $b = m$, but the second derivative with respect to $\tilde{\lambda}$, χ or m is not.

4.2 Asymmetric mass distribution

In the generic case there are six phases which are most easily classified by the arrangement of a , b , m_1 and m_K , as listed in Table 1. Of course a and b depend on the values of the parameters χ , $\tilde{\lambda}$ and the masses, which is also illustrated in Table 1.

If we fix m_1 , m_K then at most four phases can be seen by changing χ and λ . The phase boundaries are at

$$b = m_1, \quad b = m_K, \quad a = m_1, \quad a = m_K. \quad (4.12)$$

Phase	Configuration	a	b
I	$a < b < m_1 < m_K$	$(\chi - 1)\tilde{\lambda}$	$(\chi + 1)\tilde{\lambda}$
II	$a < m_1 < b < m_K$	$(\chi - 1)\tilde{\lambda}$	$\frac{\tilde{\lambda}(m_1(\chi-1)+m_K(\chi+1))}{2\tilde{\lambda}\chi+m_K-m_1}$
III	$a < m_1 < m_K < b$	$(\chi - 1)\tilde{\lambda}$	$(1 - \chi)\tilde{\lambda}$
IV	$m_1 < a < b < m_K$	$\frac{\tilde{\lambda}(m_1(\chi+1)+m_K(\chi-1))}{2\tilde{\lambda}\chi+m_K-m_1}$	$\frac{\tilde{\lambda}(m_1(\chi-1)+m_K(\chi+1))}{2\tilde{\lambda}\chi+m_K-m_1}$
II'	$m_1 < a < m_K < b$	$\frac{\tilde{\lambda}(m_1(\chi+1)+m_K(\chi-1))}{2\tilde{\lambda}\chi+m_K-m_1}$	$(1 - \chi)\tilde{\lambda}$
I'	$m_1 < m_K < a < b$	$-(\chi + 1)\tilde{\lambda}$	$(1 - \chi)\tilde{\lambda}$

Table 1: Values of a and b in all phases. Notice that not all phases are possible for all values of the masses.

The expressions for the different phase boundaries are given in Table 2 and the phase diagram in the $(\tilde{\lambda}, \chi)$ -plane for $m_1 = 1$ and $m_K = 2$ is shown in Figure 7.

Phase-boundary	Configuration	condition
$I - II$	$a < b = m_1 < m_K$	$m_1 = (\chi + 1)\tilde{\lambda}$
$II - III$	$a < m_1 < b = m_K$	$m_K = (1 - \chi)\tilde{\lambda}$
$II - IV$	$a = m_1 < b < m_K$	$m_1 = (\chi - 1)\tilde{\lambda}$
$III - II'$	$a = m_1 < m_K < b$	$m_1 = (\chi - 1)\tilde{\lambda}$
$IV - II'$	$m_1 < a < b = m_K$	$m_K = (1 - \chi)\tilde{\lambda}$
$II' - I'$	$m_1 < m_K = a < b$	$m_K = -(\chi + 1)\tilde{\lambda}$

Table 2: The phase boundaries.

It is easy to evaluate the free energy and the Wilson loop in each one of the phases, following the example in the symmetric case, and one finds once again all the phase transitions to be of third order.

5 Discussion

The purpose of this note was to study further large N limits of matrix models which arise from localization of 3d supersymmetric field theories and hence solve for their S^3 partition function. The models we studied has K fundamental fields, whose number scales with N in the limit and the novel feature that we addressed is to allow different masses for the fundamental fields.

For even K we can view our model as an ungauged version of ABJ theory with gauge group $U(N) \times U(K/2)$. In the ABJ model one would have to integrate over the Coulomb branch parameters of the $U(K/2)$ vector multiplets, but when ungauged, those get frozen into the mass distribution. An additional Vandermonde-like factor, arising from the one-loop determinant of

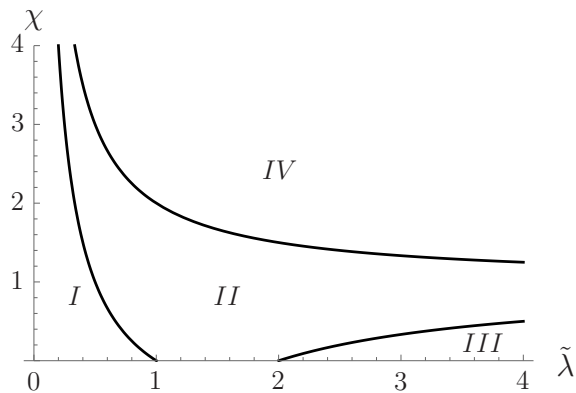


Figure 7: A phase diagram for $m_1 = 1$ and $m_K = 2$ where phases I , II , III and IV are realized. The $I - II$ boundary curve is $1 = (\chi + 1)\tilde{\lambda}$, the $II - IV$ one is given by $1 = (\chi - 1)\tilde{\lambda}$ and the $II - III$ one by $2 = (1 - \chi)\tilde{\lambda}$.

the vectors (and the Haar measure), is also absent, but could easily be incorporated as a simple determinant of the mass parameters.

We chose the simplest nontrivial mass distribution, a constant distribution over an arbitrary domain $[m_1, m_K]$, and were able to solve the matrix model in the large N limit. In fact, there is a limit of the ABJ model (and similar theories), where the eigenvalue distribution is approximately flat [24] and also in our case, we find such a solution, see Figure 1. Starting with the ABJ model in the regime where the eigenvalue distribution is flat and ungauging it, keeping one set of eigenvalues as dynamical and the other frozen, will lead to the same solution.

Therefore, we could start with the ABJ model in a different regime, where the eigenvalue distribution is not flat, ungauged one group and we are guaranteed that the solution for the other set of eigenvalues would not be modified. It would be interesting to explore others mass distributions arising in this or other ways.

We have studied the phase structure of the model and found that in the decompactification limit there are six different phases as one modifies the mass distribution, K and the Chern-Simons coupling. For finite radius spheres we found no phase transitions, but we should emphasize that our solution assumed a single cut, and while this is consistent with the numerical tests, it cannot be seen as a conclusive statement. In particular we have worked exclusively with imaginary CS parameter, which helps convergence. Our solution can be analytically continued to real values of the CS parameter, but our tests of the phase structure may no longer be valid.

Another natural generalization of our model is the case of a longer linear quiver. Such models are again easy to solve at finite N [9], and can also be written as ungauged circular quivers, which are also easy to solve at large N [7, 24]. We leave that to future work.

Acknowledgments

We are grateful to Sara Pasquetti, Jorge Russo and Kostya Zarembo for enlightening discussions. The work of L.A. is supported by the EPSRC programme grant “New Geometric Structures from String Theory”, EP/K034456/1. The work of N.D. is supported by Science & Technology Facilities Council via the consolidated grant number ST/J002798/1.

References

- [1] V. Pestun, “Localization of gauge theory on a four-sphere and supersymmetric Wilson loops,” *Commun.Math.Phys.* **313** (2012) 71–129, [arXiv:0712.2824](#).
- [2] L. F. Alday, D. Gaiotto, and Y. Tachikawa, “Liouville correlation functions from four-dimensional gauge theories,” *Lett.Math.Phys.* **91** (2010) 167–197, [arXiv:0906.3219](#).
- [3] N. Wyllard, “ A_{N-1} conformal Toda field theory correlation functions from conformal $\mathcal{N} = 2$ $SU(N)$ quiver gauge theories,” *JHEP* **11** (2009) 002, [arXiv:0907.2189](#).
- [4] A. Kapustin, B. Willett, and I. Yaakov, “Exact results for Wilson loops in superconformal Chern-Simons theories with matter,” *JHEP* **1003** (2010) 089, [arXiv:0909.4559](#).
- [5] M. Mariño and P. Putrov, “Exact results in ABJM Theory from topological strings,” *JHEP* **06** (2010) 011, [arXiv:0912.3074](#).
- [6] N. Drukker, M. Mariño, and P. Putrov, “From weak to strong coupling in ABJM theory,” *Commun. Math. Phys.* **306** (2011) 511–563, [arXiv:1007.3837](#).
- [7] M. Mariño and P. Putrov, “ABJM theory as a Fermi gas,” *J.Stat.Mech.* **1203** (2012) P03001, [arXiv:1110.4066](#).
- [8] S. Codesido, A. Grassi, and M. Mariño, “Exact results in $\mathcal{N} = 8$ Chern-Simons-matter theories and quantum geometry,” *JHEP* **07** (2015) 011, [arXiv:1409.1799](#).
- [9] S. Benvenuti and S. Pasquetti, “3D-partition functions on the sphere: Exact evaluation and mirror symmetry,” *JHEP* **05** (2012) 099, [arXiv:1105.2551](#).
- [10] A. Kapustin, B. Willett, and I. Yaakov, “Nonperturbative tests of three-dimensional dualities,” *JHEP* **10** (2010) 013, [arXiv:1003.5694](#).
- [11] A. Barranco and J. G. Russo, “Large N phase transitions in supersymmetric Chern-Simons theory with massive matter,” *JHEP* **03** (2014) 012, [arXiv:1401.3672](#).
- [12] J. G. Russo, G. A. Silva, and M. Tierz, “Supersymmetric $U(N)$ Chern-Simons-matter theory and phase transitions,” *Commun. Math. Phys.* **338** no. 3, (2015) 1411–1442, [arXiv:1407.4794](#).
- [13] M. Mariño, “Les Houches lectures on matrix models and topological strings,” [hep-th/0410165](#).
- [14] M. Mariño, “Lectures on localization and matrix models in supersymmetric Chern-Simons-matter theories,” *J. Phys.* **A44** (2011) 463001, [arXiv:1104.0783](#).
- [15] D. Gaiotto and X. Yin, “Notes on superconformal Chern-Simons-matter theories,” *JHEP* **08** (2007) 056, [arXiv:0704.3740](#).
- [16] L. Anderson and K. Zarembo, “Quantum phase transitions in mass-deformed ABJM matrix model,” *JHEP* **09** (2014) 021, [arXiv:1406.3366](#).
- [17] D. Marmiroli, “Phase structure of $\mathcal{N} = 2^*$ SYM on ellipsoids,” *JHEP* **06** (2016) 035, [arXiv:1410.4715](#).
- [18] K. Zarembo, “Strong-coupling phases of planar $\mathcal{N} = 2^*$ super-Yang-Mills theory,” *Theor. Math. Phys.* **181** no. 3, (2014) 1522–1530, [arXiv:1410.6114](#).
- [19] J. G. Russo, “ $\mathcal{N} = 2$ gauge theories and quantum phases,” *JHEP* **12** (2014) 169, [arXiv:1411.2602](#).
- [20] X. Chen-Lin and K. Zarembo, “Higher rank wilson loops in $\mathcal{N} = 2^*$ super-Yang-Mills theory,” *JHEP* **03** (2015) 147, [arXiv:1502.01942](#).

- [21] L. Anderson and J. G. Russo, “ABJM theory with mass and FI deformations and quantum phase transitions,” *JHEP* **05** (2015) 064, [arXiv:1502.06828](#).
- [22] A. Nedelin, “Phase transitions in 5D super Yang-Mills theory,” *JHEP* **07** (2015) 004, [arXiv:1502.07275](#).
- [23] J. G. Russo and M. Tierz, “Quantum phase transition in many-flavor supersymmetric QED₃,” [arXiv:1610.08527](#).
- [24] C. P. Herzog, I. R. Klebanov, S. S. Pufu, and T. Tesileanu, “Multi-matrix models and tri-Sasaki Einstein spaces,” *Phys.Rev.* **D83** (2011) 046001, [arXiv:1011.5487](#).